

Interference lithography by a soft x-ray laser beam: Nanopatterning on photoresists

A. Ritucci,^{a)} A. Reale, P. Zuppella, L. Reale, P. Tucceri, and G. Tomassetti
Physics Department of University of L'Aquila, gc-LNGS INFN, Via Vetoio, 67010 Coppito, L'Aquila, Italy

P. Bettotti and L. Pavesi
Physics Department of University of Trento, Via Sommarive 14, 38100 Povo, Trento Italy

(Received 20 May 2007; accepted 16 June 2007; published online 14 August 2007)

We have studied the feasibility of high-resolution laser interference lithography using a tabletop 46.9 nm, 1.5 ns Ar laser, combined with two different optical configurations based on a Lloyd's mirror interferometer. Using one of these schemes we have encoded periodic grating structures with a half pitch of 42 nm and a vertical modulation of 5 nm on a commercial PMMA photoresist. Experiments performed with larger half-pitch structures and detailed theoretical calculations demonstrate the potentiality of producing periodic structures with a half-pitch resolution down to 20 nm and a height of up to 60 nm. The results can be of considerable interest for the development of a complete high-resolution lithographic process operating with the 47 nm laser wavelength.

© 2007 American Institute of Physics. [DOI: [10.1063/1.2764244](https://doi.org/10.1063/1.2764244)]

I. INTRODUCTION

The ability to write periodic structures with critical dimensions (CDs) of only a few tens of nanometers has several important applications in the field of science and nanotechnology. Among these are the fabrication of semiconductor quantum dots, patterned magnetic media,¹ antireflective coatings, and distributed feedback structures for photonic crystals.² The most conventional systems used to create high-resolution structures on material surfaces on a small laboratory scale are e-beam lithography (EBL) and focused ion beams (FIBs) (see, for example, Refs. 3 and 4). The main drawback of EBL and FIB is their sequential nature. As a consequence, they are relatively slow and prone to drift, and so less useful for applications that require large areas of highly periodic lattices. In contrast, deep-ultraviolet projection lithography is suitable for the fabrication of two-dimensional (2D) structures on a large scale and can create arbitrary patterns in a single exposure step (Ref. 5 and references therein). Critical dimensions as small as 45–60 nm can be obtained with the 193 nm ArF laser and a liquid with a high refractive index located on the photoresist surface. However, optical projection lithography is extremely costly, as it requires complex optics for an aberration-free imaging of the mask and, due to the small depth of focus, a complex focusing system for the sample. Moreover, the mask has to be previously written by e-beam lithography. For this reason, optical projection lithography is justified only in the context of the semiconductor industry for high volume manufacturing of integrated circuits and it is not suitable for a small-scale research activity. However, lithographic techniques based on optical laser interference lithography (LIL) can be extremely simple, as, in principle, they need only a laser source with a sufficiently large spatial and temporal coher-

ences, a simple optical system, and no mask. In addition, due to the high depth of focus in most LIL schemes, patterns with a period down to half of the laser wavelength (about 100 nm for ArF laser) can be obtained without the need of complex alignment systems.^{1,6} With the use of an immersion liquid and the ArF laser, optical LIL can be pushed to a CD of 45 nm.

An alternative method to further improve the resolution of LIL techniques to a few tens of nanometers involves the use of coherent sources of extreme ultraviolet (EUV) and soft-x-ray radiation. However, compact coherent sources at this short wavelength region are not yet fully developed (Ref. 7 and references therein). Until now, most of the work performed with EUV and soft x rays has involved the use of large Synchrotron facilities.^{8,9} Only very recently, preliminary results have been achieved using a 46.9 nm tabletop Ar laser.¹⁰ In this paper, with the aim of optimizing the use of a 46.9 nm soft-x-ray Ar laser, in terms of the aerial image contrast and vertical modulation of the printed pattern on the photoresist, we have investigated in detail two interferometric schemes that employ Lloyd's mirror beam splitters. Using each of the schemes, we have created interferometric patterns with a half pitch down to 42 nm on commercial organic photosensitive polymer Polymethyl methacrylate (PMMA) in both single and multi-shot irradiation regimes.

II. LASER SOURCE AND PHOTORESIST

The laser source under investigation is the 46.9 nm, 1.7 ns capillary discharge Ar laser that has been developed at the University of L'Aquila producing about 0.3 mJ per single pulse at the repetition rate of 0.3 Hz. The mechanism of operation of this laser has been reported in detail previously.¹¹ The laser pulse is produced by the single pass amplification of the $3p-3s$ transition in Ne-like Ar in an elongated plasma column created by a fast capillary discharge. The geometrical characteristics of the plasma, diameter of

^{a)}Electronic mail: antonio.ritucci@tiscali.it

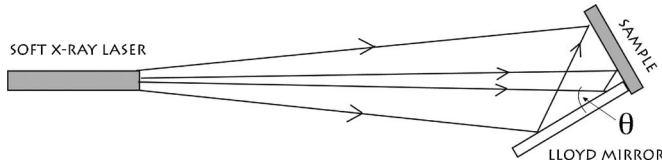


FIG. 1. Schematic of the first Lloyd mirror interferometer.

$\sim 300 \mu\text{m}$ and length of 45 cm, ensure the generation of the large spatial coherence needed for the high quality interference patterning. On the other hand, because of the lack of an optical cavity, the temporal coherence is mainly limited by the Doppler effect produced by the fast motion of ions in the plasma yielding the spectral bandwidth to $\Delta\lambda/\lambda \approx 10^{-4}$. The laser beam has an annular structure with a full divergence of 6 mrad. The mirrors in the interferometers are made from superpolished silicon with a surface roughness of 0.5 nm.

The photoresists consisted of PMMA films, molecular weight of 950 K, and spin coated onto Si substrates, typically to a thickness of 100 nm. The films were annealed at 170° for 10 min on a hot plate after coating. After EUV-IL exposure the samples were developed in a 1:3 solution of Methyl isobutyl ketone (MIBK) that is the developer and isopropanol (IPA) that prevents dissolving unexposed areas of the resist. The samples were subsequently examined using both a scanning electron microscope (SEM) and an atomic force microscope (AFM).

III. INTERFEROMETERS: THEORY AND ANALYSIS

In general, the quality and profile of interference fringes produced by two overlapping laser beams depend on the polarization of light (p or s), on the mutual degree of coherence $|\mu|$, and lastly on the relative intensities of the two beams (I_1 and I_2). When unpolarized radiation is used, the intensity of each beam is the sum of the s and p polarization components, $I_{1,2} = I_{1,2}^p + I_{1,2}^s$, and the maxima and the minima of the resulting interference fringes can be described using the following equation:

$$I = (I_1^s + I_2^s \pm 2|\mu|\sqrt{I_1^s I_2^s}) + [I_1^p + I_2^p \pm 2|\mu|\sqrt{I_1^p I_2^p} \cos(2\alpha)], \quad (1)$$

where α is half of the angle formed by the two wave vectors. The fringe period is controlled by the angle α and the laser wavelength according to the following equation:

$$P = \frac{\lambda}{2 \sin(\alpha)}. \quad (2)$$

Obviously, for an optimized fringe visibility we must fulfill the condition $I_1 \approx I_2$ with the best results expected with the s -polarized radiation. These conditions can be achieved only by a proper choice of the beam splitter and a careful optimization of its operating parameters. Because of their simplicity, we have used Lloyd's mirror beam splitters in two different experimental configurations. The first interferometric scheme (see Fig. 1) consists of a single flat grazing mirror placed along the beam path with the photoresist close to the mirror edge and orthogonal to it. Half of the laser radiation is reflected by the mirror toward the detector plane, where it interferes with the remaining direct portion of the beam. The line spacing of the interference pattern is controlled by the grazing angle (θ) according to (2), where $\alpha \approx \theta$. This method is particularly advantageous due to the simplicity of the optical system and the ease of alignment. However, as all materials experience a loss of reflectivity in the EUV range at large grazing angles, the reflected beam can become less intense than the direct one, and this results in a reduction of aerial fringe contrast according to the following equation:

$$V = 2|\mu| \frac{\sqrt{R^s(\alpha)} + \sqrt{R^p(\alpha)} \cos(2\alpha)}{2 + R^s(\alpha) + R^p(\alpha)}, \quad (3)$$

where V is the fringe visibility. If we assume that the height of the printed pattern will be proportional to the fringe visibility, this emerges as a substantial limitation of this Lloyd mirror configuration.

In order to improve the fringe visibility using our laser source, we have analyzed the scheme illustrated in Fig. 2. In this case, the Lloyd mirror can be arranged with a small grazing angle (β), while, separately, two secondary mirrors, both operating at a grazing angle $\gamma > \beta$, recombine the two beams with the suitable value of α , where $\alpha = 2\gamma - \beta$. If we configure $\beta \ll 10^\circ - 15^\circ$ for the silicon reflector, the Lloyd mirror generates two beams of comparable intensities that will interfere after the secondary mirrors and produce a pattern with the following visibility:

$$V = |\mu| \frac{R_s[(\alpha + \beta)/2] + R_p[(\alpha + \beta)/2] \cos(2\alpha)}{R_p[(\alpha + \beta)/2] + R_s[(\alpha + \beta)/2]}. \quad (4)$$

Figure 3 shows the aerial image contrast versus the half-pitch dimension calculated according to (3) and (4), having assumed a degree of coherence $|\mu| = 1$. In the case reported in Fig. 3, β was fixed to 7.5° while γ was varied. For the computation of the mirror reflectivity we have used the da-

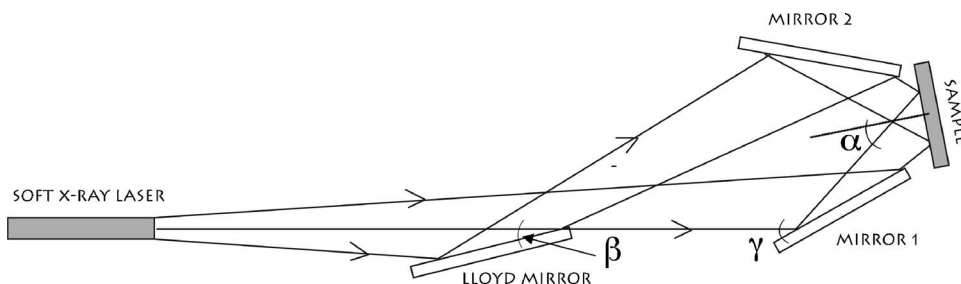


FIG. 2. Schematic of the second Lloyd mirror interferometer.

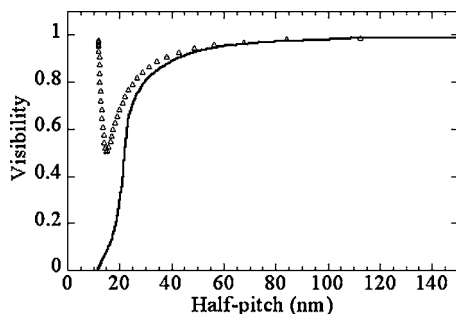


FIG. 3. Dependence of the aerial fringe visibility on the half-pitch dimension calculated for the first (solid line) and the second (empty triangles) Lloyd mirror interferometers, assuming $|\mu|=1$.

tabase of the Center of X-ray Optics (Ref. 12) at $\lambda=41$ nm and considered silicon reflectors with a 3 nm thick SiO_2 layer on the top. We can see that, at the half pitch of 20 nm, V reduces to about 25% in the first scheme, while, in the second scheme, V is expected to remain $>70\%$ at the same half pitch. Moreover in this scheme, V returns toward unity below 15 nm due to the beneficial removal of the p -polarized component through the secondary mirror reflection. It is important to notice that the use of such schemes is made possible only if the coherence properties of the laser beam are sufficiently high. The coherence properties determine the transverse extension of the printable patterns, respectively, to be $L_T/2 \sin(\alpha)$ and/or to $L_S/2 \cos(\alpha)$ where L_T and L_S are the temporal and the spatial coherence lengths, respectively. The temporal coherence length is determined by the spectral bandwidth of the radiation according to $L_T \approx \lambda^2/\Delta\lambda$, and that for our laser is ≈ 0.4 mm. The spatial coherence has been characterized in detail in previous experiments.^{13,14} Extrapolating the data reported in Ref. 14 to our 45 cm laser amplifier, we expect a transverse coherence length of ~ 4.5 mm at 1 m from the capillary output. A larger transverse coherence can be obtained by moving further away from the capillary output. With some degree of approximation, Fig. 4 shows the maximum number of fringes obtainable with our laser as a function of the half-pitch dimension. For half-pitch structures smaller than 100 nm, the total number of lines will be mostly controlled by the temporal coherence to about $L_T/\lambda \approx 10^4$ which is a suitable number for several different applications, i.e., the testing of new photoresists for the next gen-

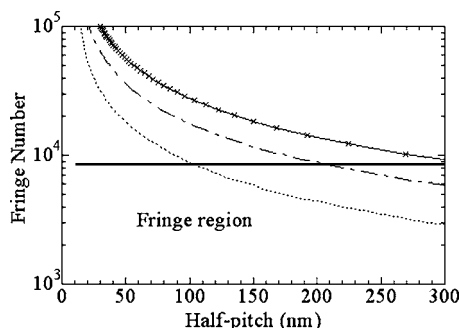


FIG. 4. Limitations on the maximum number of fringes vs the half pitch imposed by the temporal coherence length of 0.4 mm (solid line) and by different values of the spatial coherence length: 4.5 mm (dotted line), 9 mm (dashed line), and 13 mm (crossed line).

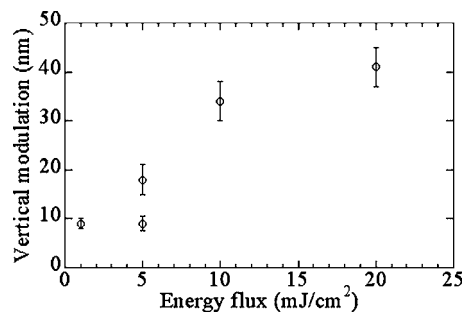


FIG. 5. Dependence of the vertical modulation of patterns with a half pitch of 600 nm on the illumination dose.

eration EUV projection lithography that will soon reach the 22 nm production node.

IV. EXPERIMENTAL RESULTS AND DISCUSSION

A large aerial image contrast is not a sufficient condition for the successful development of a full lithographic process, which includes pattern imprinting on the resist and the pattern transfer from the polymer to the substrate. At $\lambda=46.9$ nm we are in the critical situation where the polymer absorbs the laser light with a characteristic penetration depth of less than 20 nm. As a consequence, one can expect to achieve a low vertical modulation of the pattern on the developed photoresist which is undesirable. To obtain acceptable results, it is necessary to carefully optimize several other parameters such as the resist composition and thickness, the photoresist development procedure, and the illumination dose.¹⁵

We first evaluated the maximum vertical modulation achievable on the PMMA under optimized conditions of aerial image contrast, mechanical stability of the setup, and photoresist resolution. To perform this analysis, we have written several patterns using a relatively large period (>1000 nm) and have varied the illumination dose. Due to its simplicity, we used the first interferometric scheme.

Figure 5 shows the dependence of the pattern modulation on the radiation dose for a grating with a period of 1200 nm. A single laser shot delivers an energy flux of ~ 1 mJ/cm² over an area of 20 mm². It can be observed that this flux is large enough to impress the photoresist and create a vertical modulation of 9 nm. This modulation increases with the energy flux and at ~ 20 mJ/cm², i.e., about 20 laser shots, we observed a height of 45 nm. Despite the large period, this vertical modulation is still limited by the mechanical vibration. In fact, at larger fringe periods (>2.5 μm) we observed a further increase of the modulation height up to 60 nm. These results point to the fact that with an optimized PMMA thickness of several tens of nanometers it is possible to create patterns where lines of polymer alternate with the silicon substrate.

The second goal of the experiment was to shrink down the pattern resolution to below 50 nm and to compare the structures printed with the two different interference schemes. Figures 6(a) and 6(b) show quite good patterning on the PMMA with a half-pitch resolution of 100 nm produced by the first Lloyd's mirror configuration again with 1

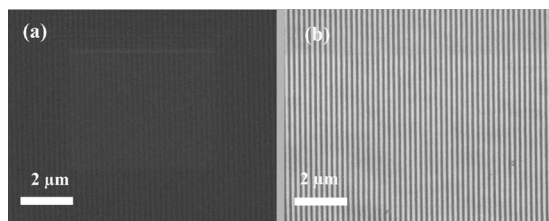


FIG. 6. SEM images of patterns impressed with the first Lloyd mirror configuration having the half pitch of 100 nm. The patterns were obtained with (a) ~ 1 mJ/cm² (single laser shot) and (b) ~ 20 mJ/cm² (20 laser shots).

and 20 laser pulses, respectively. But, at smaller periods, the height and the quality of the fringes drop substantially. At the half pitch of 51 nm, the vertical modulation at 20 mJ/cm² has already reduced to 15–16 nm.

Figures 7(a) and 7(b) demonstrate the creation of grating structures with a half pitch of 42 nm obtained both with the first [7(a)] and the second [7(b)] Lloyd's mirror configurations. This figure compares both the pattern quality and the vertical modulation. Even if the strong mechanical vibrations of our optical setup do not allow a direct comparison of the experimental data with the theoretical trends reported in Fig. 3, we can appreciate a significant difference between the two configurations: a modulation of ~ 4 –5 nm obtained with the second scheme, compared to that below 1.5 nm measured with the first scheme. Despite the low vertical modulation of the patterns achieved up to now, the experimental results are quite encouraging and represent a good starting point for the creation of a reliable, simple, and inexpensive lithographic scheme capable of printing patterns with feature sizes well below 50 nm.

V. CONCLUSIONS

In conclusion, we have reported preliminary results concerning the use of a 46.9 nm laser beam in a high-resolution

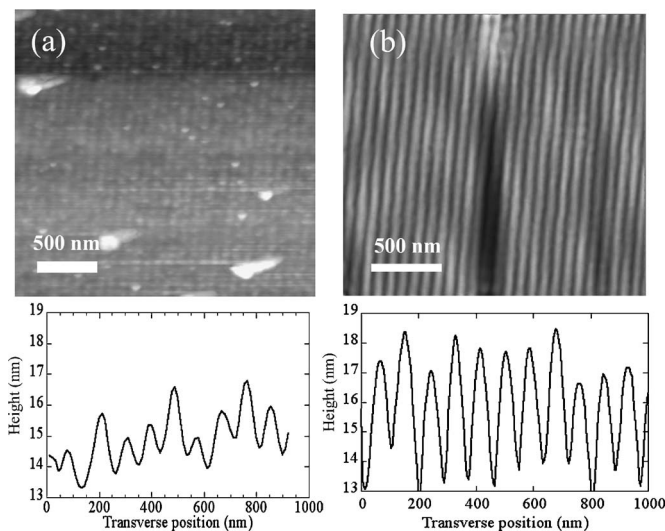


FIG. 7. AFM images and corresponding plot profiles of 42 nm half-pitch structures printed with the first (a) and the second (b) Lloyd mirror configurations, respectively.

interference lithography process. Two different experimental schemes based on Lloyd's mirror beam splitters have been investigated. We have found that a simple maskless scheme based on a Lloyd mirror beam splitter and two secondary grazing reflections has the potential to produce large aerial image contrast ($>50\%$) for half-pitch structures as low as 15 nm. From the experimental point of view, both schemes have been used to print patterns with half-pitch down to 42 nm. We have demonstrated the possibility of writing high-resolution periodic structures in commercial PMMA resists using the 46.9 nm wavelength radiation.

The vertical modulation obtained on the resist layer, about 60 nm at half-pitch of 1.2 μ m, decreases with reducing the feature size, but nevertheless, by improving the mechanical stability of the setup and the resist chemistry, the development of resist layers with a thickness comparable to those employed in classical lithographic methods should easily be achieved.

It should be noticed that the approach of using short wavelength electromagnetic radiation has a considerable advantage over the use of an electron beam. With the EBL, proximity effects and the serial nature of the technique are the main limiting factors in achieving high resolutions over large areas and in short exposure times. Due to its simplicity and its parallel patterning modality, the EUV based lithographic method can guarantee a larger throughput and comparable resolution over wider areas. For this reason it could find important applications in nanofabrication processes.

ACKNOWLEDGMENTS

The work has been supported by the National Institute of Nuclear Physics and Provincia Autonoma di Trento. The authors acknowledge useful discussions with Professor P. Dunne.

- ¹S. R. J. Brueck, Proc. IEEE **93**, 1704 (2005).
- ²H. Schiff, S. Park, B. Y. Jung, C. G. Choi, C. S. Kee, S. P. Han, K. B. Yoon, and J. Gobrecht, Nanotechnology **16**, S261 (2005).
- ³J. Joo, B. Y. Chow, and J. M. Jacobson, Nano Lett. **6**, 2021 (2006).
- ⁴W. X. Li, G. Lalev, S. Dimov, H. Zhao, and D. T. Pham, Appl. Surf. Sci. **253**, 3608 (2007).
- ⁵Proceedings of the fifth EUVL Symposium Barcelona, Spain 15–18 October 2006 (unpublished).
- ⁶J. A. Hoffnagle, W. D. Hinsberg, M. Sanchez, and F. A. Houle, J. Vac. Sci. Technol. B **17**, 3306 (1999).
- ⁷H. Daido, Rep. Prog. Phys. **65**, 1513 (2002).
- ⁸H. H. Solak, J. Phys. D **39**, R171 (2006).
- ⁹E. Di Fabrizio *et al.*, J. Phys.: Condens. Matter **16**, S3517 (2004).
- ¹⁰M. G. Capeluto *et al.*, IEEE Trans. Nanotechnol. **5**, 3 (2006).
- ¹¹G. Tomassetti *et al.*, Opt. Commun. **231**, 403 (2004).
- ¹²Website: <https://www.cxro-lbl.gov>
- ¹³Y. Liu, M. Seminario, F. G. Tomasel, C. Chang, J. Rocca, and D. Attwood, Phys. Rev. A **63**, 033802 (2001).
- ¹⁴A. Ritucci, G. Tomassetti, A. Reale, F. Flora, and L. Mezi, Phys. Rev. A **70**, 023818 (2004).
- ¹⁵R. Gronheid, H. H. Solak, Y. Ekinici, A. Jouve, and F. Van Roey, Microelectron. Eng. **83**, 1103 (2006).